Motion parallax for object localization in electric fields

Kevin Hunke[1], Jacob Engelmann[2], Hanno Gerd Meyer[1] and Axel Schneider[1]

[1] Biomechatronics Group, Faculty of Engineering and Mathematics, University of Applied Sciences, Bielefeld, Germany
[2] Active Sensing, Faculty of Biology, Bielefeld University, Bielefeld, Germany

E-mail: kevin.hunke@fh-bielefeld.de, jacob.engelmann@uni-bielefeld.de, hanno_gerd.meyer@fh-bielefeld.de, axel.schneider@fh-bielefeld.de

Abstract. Parallax, as a visual effect, is used for depth perception of objects. But is there also the effect of parallax in the context of electric field imagery? In this work, the example of weakly electric fish is used to investigate how the self-generated electric field that these fish utilize for orientation and communication alike, may be used as a template to define electric parallax. The skin of the electric fish possesses a vast amount of electroreceptors that detect the self-emitted dipole-like electric field. In this work, the weakly electric fish is abstracted as an electric dipole with a senor line in between the two emitters. With an analytical description of the object distortion for a uniform electric field, the distortion in a dipole-like field is simplified and simulated. On the basis of this simulation, the parallax effect could be demonstrated in electric field images i.e. by closer inspection of voltage profiles on the sensor line. Therefore, electric parallax can be defined as the relative movement of a signal feature of the voltage profile (here, the maximum or peak of the voltage profile) that travels along the sensor line (peak trace, PT). The PT width correlates with the object's vertical distance to the sensor line, as close objects create a large PT and distant objects a small PT, comparable with the effect of visual motion parallax.

Keywords: motion parallax, electric field, object localization, weakly electric fish, electroreceptor, electrolocation, field simulation

Submitted to: *Bioinspir. Biomim.*

1. Introduction

Depth perception is created by many sources of information. For example it can be based on the visual perspective and the texture of an object. The human eye creates two-dimensional depth information on the retina. The optics of the human eye project the outside world on a 2D surface. One way to extract depth from this, i.e. a transformation back to 3D, is to move the image over the retina. Through this movement visual motion parallax is induced. Nearby objects pass the field of view quicker than more distant objects, that thus appear to move more slowly. For example looking out a side window of a moving train or car, nearby objects appear to rush by, whereas objects that are farther away appear to move slower. Additionally, the relative movement also induces differences in the apparent movement direction: when looking at a fixed point, objects farther and closer from this fixation point appear to move in opposite directions. The experimental study of motion parallax dates back to the time of von Helmholtz (1925), who provided a description of the retinal transformations produced by the movement of an observer [1].

The effect of motion parallax is illustrated in figure 1 by two different objects and their movement on the retina as the eye does a side-wards shift to the right without rotating. The image of the closer object B moves all the way across the retina from S to B, as indicated in red. The more distant object A moves from S to A on the retina (blue). As the image of the closer object B travels a larger distance across the retina than object A, it appears to move more quickly in the same amount of time [2]. Therefore, motion parallax is the relative movement of an image across the retina as either the observer or the object translates across the field of view.

The concept of motion parallax for depth perception has also been applied in biomimetic approaches. For example, heuristics derived from visual parallax of blowflies were successfully implemented in a mechanical robot that navigates through the environment by determining the distance to obstacles by ego-motion evoked visual parallax [3].

Also some fish species, for instance *Gnathonemus petersii* (Peters' elephant-nose fish), have the ability to detect objects in their environment by sensing the environmentally induced modulations of their actively generated electric field. In this species, the localization range is about twice the animals body length [4]. The fish is able to orient in darkness or turbid waters and to classify unknown objects with respect to size, shape, material, vertical distance and lateral displacement [5]. The electric field is generated by specialized muscle cells located in the tail shaft of these fish [6]. Through synchronized discharges of this electric organ (EOD, electric organ discharge) the fish build up a dipole-like electric field surrounding their body. Electroreceptors, so called *mormyromasts*, are distributed across the fish's skin and locally measure the properties (amplitude and waveform-alteration) of the field [7]. The electroreceptors in the skin enable fish to measure potential changes in the range of 0.1 % of the basal field amplitude on the skin surface [8]. Recent studies suggest that, comparable to the ego-motion induced visual parallax in blowflies, weakly electric fish use sophisticated movement patterns (*va-et-vient and B-scans,* [9, 10]) that can induce depth cues (electric parallax) [11]. This work extends on the above hypothesis to provide a theoretic and analytic framework to analyze

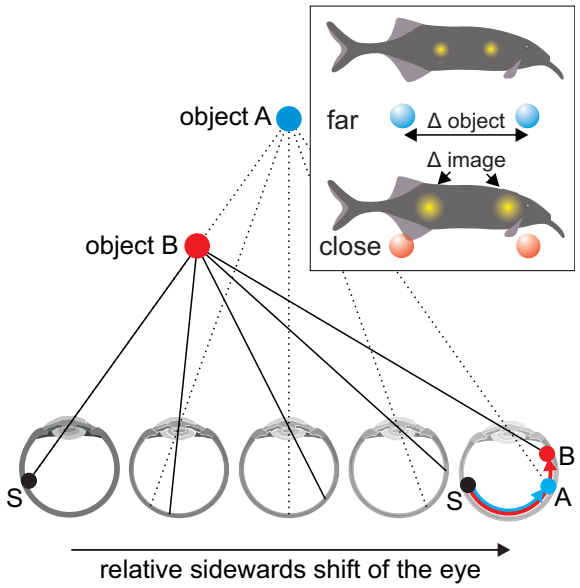

Figure 1. Illustration of the effect of relative movement between the human eye and two objects at different distance. Because object B is closer to the observer, its image moves farther across the retina (S to B) than the image of the object A (S to A), as illustrated by the red and blue trace on the right retina. The inset on the top right shows a similar effect of motion parallax for the weakly electric fish. Close objects generate a larger Δimage than farther ones for the same object movement Δobject.

the extend to which electric parallax may be used, both in biological organisms, but as a perspective, also for electrosensory-guided autonomous agents. It must be emphasised, however, that the model character of the electric fish for the modelling of the electric field in this work is rather loosely chosen. As can be seen in the following, a simple electric dipole is assumed as the source system and the sensory system consists only of measurement locations along a straight line, representing a one-dimensional sensor array that measures potentials (potential differences between neighbouring electrodes). The use of potential measurements instead of direct electric field measures for the formulation of parallax was chosen deliberately to emphasise that the sensor phenomenon is in the spotlight of this work. This system described was chosen to enable a first approach for the parallax formulations that is as straightforward as possible.

2. Parallax formulation based on an electric dipole

For simple geometric objects like spheres or cylinders within an electric field, an analytical description for the field distortion due to the presence of objects can be found. The analytical description presented in this section is based on Maxwell's equations and the corresponding conditions at a surface interface between different media, e.g. fluid and object. Based on this analytical description, a simulation is later set up that describes field distortions and potential changes in the area of an imaginary sensor line. From the simulated measured values (voltage profile) on the sensor line, features will be developed that are suitable for parallax observation.

The approach presented in the following sections is based on an initial work by Rasnow [12]. Before details are provided, a brief summary of different approaches, that researchers have taken to understand and abstract the sensory capabilities of weakly electric fish, is given. This is to make it easier for the reader to follow the analysis and conclusions in this work.

Early on, Lissmann and Machin [13] provided an analytical framework to derive the effect of objects in the electric field generated by these fish. The change of the field geometry around the animal was presented in which several key concepts were provided: A distinction between the field in absence of objects (basal field) and the object-perturbed field. The change in the electric field along the animal's body imposed by an object is equal to the potential generated by the perturbing field. This change depends on the field, the object, and the properties of the animals body and has been termed the "electric image" of an object (see for example [14]). For simple objects of known electrical properties this effect may be simulated by calculating the potential change over the animal's sensors analytically using Maxwell's equations (see section 2.2). Accordingly, the electric images can be modelled either as the perturbation of the electric field due to an object as an essential field phenomenon, or as the resulting electric potential at the skin [12]. The electric field is the negative gradient of the electric potential, but while the electric field at any given point has a unique value (amplitude and angle), the electric potential depends on the chosen reference point. Nonetheless, the calculation of the local electric potential has frequently been used to provide fast simulations of electric images in order to reach an abstract understanding of active electric imaging [12, 15, 16]. In addition, the existing models predominantly have focused on the amplitude of the electric field and associated images. To come closer to the biological template, the electric properties of the skin and internal tissue of the animal need to be incorporated and this has been achieved using numerical rather than analytical approaches like finite-element or boundary-element methods [17, 18, 19, 20]. Similar to the majority of published approaches, this work will focus on electric images based on the potential amplitude. However, weakly electric fish can additionally use phase changes of the self-generated field to acquire sensory information [21] and these have also been modelled in detail [22].

In order to provide a theoretical and analytic framework to address to which extend the concept of electric parallax may be used to understand the biological templates behavior better, as well as to gain insights as to the suitability of this concept for electrosensory-guided autonomous agents, here the complexity of the approach is reduced by use of an analytical model that focuses on the local field potential.

2.1. Analytical description of electric fields

In this work, two different field characteristics, a uniform electric field and an electric dipole field, are considered. The description of the uniform electric field itself is simple and the interaction of field and basic geometrical object (e.g. sphere) can also be solved analytically to describe the resulting field distortions as for example shown by [12] (for a comprehensive description of electric fields in the context of biological tissues see [23]). Under certain restrictions, the results of the distorted uniform field can be used to determine the distortions of the dipole field as well.

2.1.1. Uniform electric field

A uniform electric field with the electric field strength vector $\vec{E}$ has always the same direction, orientation

and magnitude at each point in space. An example for a uniform electric field is the field of two oppositely charged plates in space. The field strength $\vec{E}$ is perpendicular to the plate surfaces and it points from the positively charged to the negatively charged plate, as depicted in figure 2(a). The electric field strength $\vec{E}$ between two oppositely charged plates is proportional to the amount of charge Q, inversely proportional to the area A of the plates and depends on the vacuum permittivity ϵ_0 as described equation (1).

$$E = \frac{1}{\epsilon_0} \cdot \frac{|Q|}{A} = \frac{F_{el}}{|q|} \quad \text{with } \epsilon_0 = 8,854 \cdot 10^{-12} \frac{As}{Vm} \tag{1}$$

At the same time the electric field strength exerts a force F_{el} on an introduced sample charge q. The potential φ in the uniform electric field of two oppositely charged plates is proportional to the electric field strength E and to the distance x of a point in the inter space to the negatively charged plate. It is calculated by equation (2).

$$\varphi(x) = E \cdot x \tag{2}$$

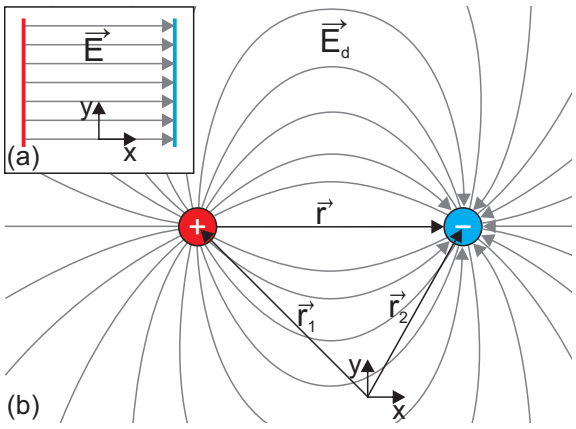

Figure 2. Illustration of electric field lines. A uniform electric field (a) with the field strength $\vec{E}$ in x-direction is shown. The field lines point away from the positively charged plate towards the negatively charged plate. The magnitude E of the electric field is constant and the field lines point in the same direction and have the same space between each other. In (b) an electric field of a dipole is shown with its position vectors $\vec{r}_1$ and $\vec{r}_2$ for the point charges.

2.1.2. Electric dipole field

In the simplest case, the electric dipole field is formed by two charges q_1 and q_2 located in an empty space, as shown in figure 2(b). For this situation, the Coulomb force F_c can be calculated by equation (3).

$$F_c = \frac{1}{4\pi\epsilon_0} \cdot \frac{q_1 \cdot q_2}{r^2} \tag{3}$$
$$\text{with} \quad r = |\vec{r}_1 - \vec{r}_2| \quad \text{and} \quad \vec{r} = \vec{r}_1 - \vec{r}_2$$

The vectorial notation of discrete charges provides the Coulomb force field where a charge q_1 is exposed to the field of a second charge q_2 and vice versa. The position vectors $\vec{r}_1$ and $\vec{r}_2$ of the two charge centers are shown in figure 2(b) and were used in equation (4) to calculate the Coulomb force vector $\vec{F}_c$.

$$\vec{F}_c = \frac{1}{4\pi\epsilon_0} \cdot \frac{q_1 \cdot q_2}{|\vec{r}_1 - \vec{r}_2|^2} \cdot \frac{\vec{r}_1 - \vec{r}_2}{|\vec{r}_1 - \vec{r}_2|} \tag{4}$$

The electric field strength is a vectorial quantity and is defined as the quotient of the Coulomb force acting on a positively charged sample at a certain point of the field and the charge of the sample.

$$\vec{E} = \frac{\vec{F}_c}{q} \qquad \text{with} \quad q = q_1 \vee q_2 \tag{5}$$

The combination of equation (4) and (5) results in equation (6) as an electric field of a point charge.

$$\vec{E}(\vec{r}) = \frac{1}{4\pi\epsilon_0} \cdot \frac{q}{|\vec{r} - \vec{r}_q|^3} \cdot (\vec{r} - \vec{r}_q) \tag{6}$$

As in the case of an electric dipole for parallax formulation, the superposition principle applies to multiple point charges. The resulting electric dipole field $\vec{E}_d$ is formulated in equation (7).

$$\vec{E}_d(\vec{r}) = \sum_{k=1}^{N} \frac{1}{4\pi\epsilon_0} \cdot \frac{q_k}{|\vec{r} - \vec{r}_k|^3} \cdot (\vec{r} - \vec{r}_k) \tag{7}$$

Besides the electric field $\vec{E}$, the electrostatic potential φ will also be required for the definition of the electric parallax later on. The relationship between the electric field and the potential is given by equation (8).

$$\vec{E} = -\vec{\nabla}\varphi \tag{8}$$

With the electric field for a point charge in equation (6) and the relation given in equation (8) the potential of a point charge can be calculated by:

$$\varphi(\vec{r}) = -\int_0^\infty \vec{E} \cdot d\vec{r} = -\frac{1}{4\pi\epsilon_0} \int_0^\infty \frac{q}{r^2} \cdot dr \tag{9}$$

The potential $\varphi(\vec{r})$ results from a line integral of the electric field from zero to infinity by moving a test charge from the electric field of the charge to infinity. The solution of the line integral results in equation (10).

$$\varphi(\vec{r}) = \frac{1}{4\pi\epsilon_0} \cdot \frac{q}{|\vec{r} - \vec{r}_q|} \tag{10}$$

The electrostatic potential of a dipole φ_d is given by superposition of equation (10) for two charges. The charges q_1 and q_2 in equation (11) have opposite polarity but the same magnitude.

$$\varphi_d(\vec{r}) = \frac{q_{1,2}}{4\pi\epsilon_0} \cdot \left[\frac{1}{|\vec{r} - \vec{r}_{q1}|} - \frac{1}{|\vec{r} - \vec{r}_{q2}|} \right] \tag{11}$$

2.2. Perturbation by round objects

For the later consideration of moving objects in the context of parallax, simple geometrical objects have to be integrated into the field scenario in the next step. This work focuses on round objects. The resulting distortion of the electric field is to be described analytically.

2.2.1. Round object in a uniform electric field

To find an analytical description for the field distortion due to a round object in a uniform field, as shown in figure 3, a solution of the Poisson's equation must be found. The Poisson's equation (12) results from equation (8) and the first Maxwell equation ($\vec{\nabla} \cdot \vec{D} = \rho_q$, differential form of Gauss's law) by applying the divergence to the electric displacement field $\vec{D}$.

$$\Delta\varphi = -\frac{\rho_q}{\epsilon} \tag{12}$$

A solution of the Poisson's equation (12) can be found by calculating the electric potential φ for a given charge density ρ_q and the permittivity ϵ of a medium. For the purpose in this work, the charge density distribution is assumed to be zero, since there are no free charges in the space. This results in Laplace's equation (13).

$$\Delta\varphi = 0 \tag{13}$$

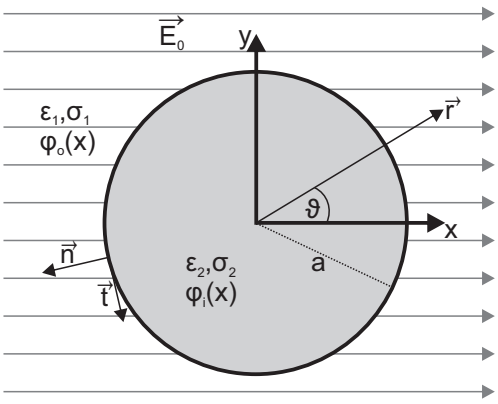

Figure 3. Round object in a uniform electric field $\vec{E}_0$. The field is aligned with the x-axis in horizontal direction. At the origin of the coordinate system, an object with radius a, permittivity ϵ_2 and conductivity σ_2 is placed in a medium with permittivity ϵ_1 and conductivity σ_1. ϑ represents the angle between the initial electric field $\vec{E}_0$ and vector $\vec{r}$.

Due to the rotational symmetric object in the arrangement in figure 3, a description in spherical coordinates (r, ϑ, ϕ) seems appropriate for the mathematical solution. Since this work deals with a 2D round object instead of a 3D sphere, the solution only depends on one of the two angles (ϑ) and is independent of the other (ϕ). In addition, the initial uniform electric field is aligned horizontally with the x-axis and has a magnitude of E_0. For this configuration, equation (13) can be solved by means of Legendre polynomials. The general solution for Laplace's equation (13) with Legendre polynomials $P_l(\cos\vartheta)$ has been presented e.g. by Jackson [24] and is shown in equation (14). The coefficients A_l and B_l can be determined by examination of the interface between external medium and object as given in figure 3.

$$\varphi(r,\vartheta) = \sum_{l=0}^{\infty} \left[A_l r^l + B_l r^{-(l+1)} \right] P_l(\cos\vartheta) \tag{14}$$

Suppose that the potential on the surface of a round object of radius a is equal to $\varphi(r,\vartheta)$, and it is required to find the potential φ_i inside the sphere ($r < a$). If there are no charges at the origin, the potential must also be finite at the origin. Therefore, only positive powers of r should occur in equation (14), since otherwise, r approaching zero led to an infinite potential. This results in equation (15).

$$\varphi_i(r,\vartheta) = A_1 r P_1(\cos\vartheta) + \sum_{l=0, l\neq 1}^{\infty} A_l r^l P_l(\cos\vartheta) \tag{15}$$

Outside the round object ($r > a$), the potential of the uniform electric field according to equation (2) is present. The electric field distortion due to the round object is achieved by applying equation (14) in addition to the potential of the uniform field (superposition). Since the field distorting effect of the object decreases with increasing radius r, only the negative powers of r are used this time, as shown in equation (16).

$$\varphi_o(r,\vartheta) = -E_0 x + \sum_{l=0}^{\infty} B_l r^{-(l+1)} P_l(\cos\vartheta) \tag{16}$$

Note, that the potential in the uniform electric field solely changes in x-direction. Therefore, x can be replaced by $x = r\cos\vartheta = rP_1(\cos\vartheta)$. This results in:

$$\varphi_o(r,\vartheta) = (-E_0 r + B_1 r^{-2}) P_1(\cos\vartheta) + \sum_{l=0, l\neq 1}^{\infty} B_l r^{-(l+1)} P_l(\cos\vartheta) \tag{17}$$

In both potential equations (15) and (17), the term for $l = 1$ is extracted from the sum, which seems to be arbitrary but will be used in the next steps.

Determination of the coefficients

To determine the coefficients A_l and B_l, additional boundary conditions are needed. First, the potential at the interface between two different media is continuous, as shown in figure 3. If the potential at the surface of the round object would change abruptly, the electric field would be infinite at this location. Therefore, $\varphi_o(a,\vartheta) = \varphi_i(a,\vartheta)$ must apply. By setting equation

(15) and (17) equal to each other for $r = a$, this results in:

$$(-E_0 a + B_1 a^{-2})P_1(\cos\vartheta) + \sum_{l=0,l\neq 1}^{\infty} B_l a^{-(l+1)} P_l(\cos\vartheta) = A_1 a P_1(\cos\vartheta) \quad + \sum_{l=0,l\neq 1}^{\infty} A_l a^l P_l(\cos\vartheta) \quad (18)$$

Since the Legendre polynomials P_l are an orthogonal system of functions and thus linearly independent, it follows that coefficients with the same l must be the same on both sides of the equation:

$$B_l a^{-l-1} = A_l a^l \qquad \text{for} \quad l \neq 1 \qquad (19a)$$

$$-E_0 a + B_1 a^{-2} = A_1 a \qquad \text{for} \quad l = 1 \qquad (19b)$$

The equations (19a) and (19b) are not yet sufficient to determine the coefficients A_l and B_l. Additional boundary value conditions are required. At the boundary surface between round object and external medium, the tangential and normal components of the electric field $\vec{E}$ as well as of the displacement field $\vec{D}$ are assumed to be continuous when crossing the boundary from inside to outside and vice versa. The normal component of the electric field is aligned with the vector $\vec{r}$ and points away from the origin in radial direction. Therefore, as additional boundary condition, the derivation of the inner potential and the outer potential along the normal to the boundary surface is assumed to be equal. This results in the boundary condition (20) at the surface of the object ($r = a$).

$$(\sigma_1 + j\omega\epsilon_1)\frac{\partial\varphi_o}{\partial r}\bigg|_{r=a} = (\sigma_2 + j\omega\epsilon_2)\frac{\partial\varphi_i}{\partial r}\bigg|_{r=a} \qquad (20)$$

Due to the presence of dielectrics, equation (20) also contains material parameters for the medium (σ_1, ϵ_1) and object (σ_2, ϵ_2). Using the derivatives of equation (15) and (17) with the substitution $\Psi_{1,2} = (\sigma_{1,2} + j\omega\epsilon_{1,2})$ for the material parameters in equation (20) results in:

$$\Psi_1(-E_0 - 2B_1 a^{-3})P_1(\cos\vartheta) + \sum_{l=0,l\neq 1}^{\infty} \Psi_1 B_l(-l-1)a^{-l-2}P_l(\cos\vartheta) = \Psi_2 A_1 P_1(\cos\vartheta) + \sum_{l=0,l\neq 1}^{\infty} \Psi_2 A_l l a^{l-1} P_l(\cos\vartheta) \qquad (21)$$

Again, the coefficients with the same l must be the same on both sides, which results in:

$$\Psi_1 B_l(-l-1)a^{-l-2} = \Psi_2 A_l l a^{l-1} \qquad \text{for} \quad l \neq 1 \qquad (22a)$$

$$\Psi_1(-E_0 - 2B_1 a^{-3}) = \Psi_2 A_1 \qquad \text{for} \quad l = 1 \qquad (22b)$$

The coefficients can now be determined from equations (19a,b) and (22a,b). By inserting (19a) in (22a) follows $B_l \cdot (-\Psi_1 l - \Psi_1 - \Psi_2 l) = 0$ for $l \neq 1$, which can only be solved by $B_l = 0$ and thus also $A_l = 0$. By inserting (19b) in (22b), A_1 and B_1 can be calculated as shown in equation (23a) and (23b), respectively. χ and Γ have been introduced for the simplification of writing and are called contrast factors.

$$A_1 = -E_0\frac{3}{2+\Gamma} \quad \text{with } \Gamma = \frac{\sigma_2 + j\omega\epsilon_2}{\sigma_1 + j\omega\epsilon_1} \qquad (23a)$$

$$B_1 = E_0 a^3 \chi \quad \text{with } \chi = \frac{\sigma_2 - \sigma_1 + j\omega(\epsilon_2 - \epsilon_1)}{\sigma_2 + 2\sigma_1 + j\omega(\epsilon_2 + 2\epsilon_1)} \qquad (23b)$$

The contrast factor χ is unity for a perfect conductor ($\chi = 1$), $\chi = -0.5$ for a perfect insulator and zero ($\chi = 0$) if the electrical impedance of the object matches that of the surrounding medium.

Potential inside the round object

According to the coefficient A_1 and equation (15), the potential inside the round object can be described as:

$$\varphi_i(r,\vartheta) = \left(-E_0\frac{3}{2+\Gamma}\right) r P_1(\cos\vartheta) = -\left(\frac{3}{2+\Gamma}\right)\vec{E}_0 \cdot \vec{r} \qquad (24)$$

Equation (24) shows, that only the second contrast factor Γ, which defines the relationship between the material parameters, characterizes the potential inside the object. In perfect conductors, the electrical induction causes the electric field inside the object to be zero and the potential at the boundary to be constant. In perfect dielectrics, an electric field can be found on the surface and inside the object due to the polarization charge, which is opposed to the applied field.

Potential outside the round object

According to the coefficient B_1 and equation (17), the potential outside a round object can be described as:

$$\varphi_o(r,\vartheta) = (-E_0 r + E_0 a^3 \chi r^{-2})P_1(\cos\vartheta) = -E_0 x \; + E_0\frac{a^3}{r^2}\cos\vartheta \cdot \chi = \varphi_0(\vec{r}) \; + \delta\varphi(\vec{r}) \qquad (25)$$

Equation (25) represents the analytical description of the distortion caused by a round object (second term) in a uniform electric field (first term). It shows that the charge separation is always responsible for a disturbing object becoming an electric dipole. The field distortion in equation (25) (second term) can also be written in vector notation (see Rasnow [12]) as shown in equation (26).

$$\delta\varphi(\vec{r}) = \vec{E}_0\vec{r}\left(\frac{a}{|\vec{r}|}\right)^3 \frac{\sigma_2 - \sigma_1 + j\omega(\epsilon_2 - \epsilon_1)}{\sigma_2 + 2\sigma_1 + j\omega(\epsilon_2 + 2\epsilon_1)} \qquad (26)$$

2.2.2. Round object in an electric dipole field

To find an analytical description for the field distortion due to a round object in a dipole field, the solution of Poisson's equation is more complex than in the case of the uniform field. Therefore, this work takes a less complex approach by making the simplifying assumptions that a) the object is small and b) that the field in the vicinity of the object is uniform with a constant field strength E as shown in figure 4. However, the direction of the local uniform field vector $\vec{E}$ is aligned with the direction of the field of the underlying dipole field at that location.

As shown in figure 4, ϑ is the angle between the direction of the (underlying) field direction and the vector $\vec{r}$. The potential outside the object results from the superposition of the dipole potential (equation (11)) and by the distortion potential of the object (equation (26)).

$$\varphi_o(\vec{r}) = \varphi_d(\vec{r}) + \delta\varphi(\vec{r})$$
$$= \frac{q_{1,2}}{4\pi\epsilon_1}\left(\frac{1}{|\vec{r}-\vec{r}_{q1}|} - \frac{1}{|\vec{r}-\vec{r}_{q2}|}\right) + \vec{E}_d\vec{r}\left(\frac{a}{|\vec{r}|}\right)^3\chi \quad (27)$$

Equation (27) shows the potential of the dipole field with the object perturbation. As in the uniform electric field the charge separation is responsible for the object becoming an electric dipole. The analytical description of a round object distorting a dipole field from equation (27) is used to simulate the potential at the location of a sensor/sensor line in the next sections.

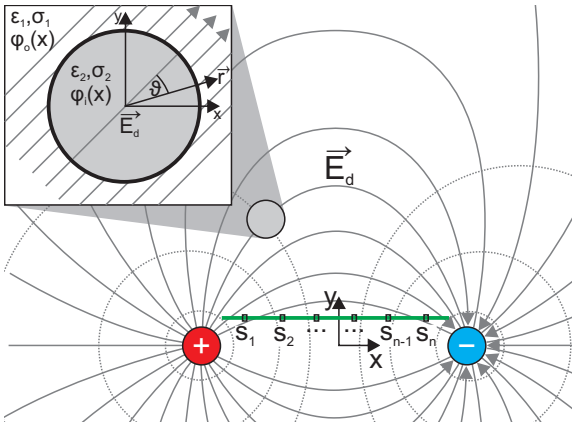

Figure 4. Schematic illustration of the active sensor, consists of a sensor line (green), assumed with n sensor locations, within an electric dipole field. A round object, with radius a, is placed in the dipole field $\vec{E}_d$. The field near the object is assumed to be uniform. The presence of dielectrics in the medium (ϵ_1,σ_1) and of the object (ϵ_2,σ_2) are shown. ϑ represents the angle between the dipole field $\vec{E}_d$ and vector $\vec{r}$.

2.3. Active sensor composed of sensor line and electric dipole

As a first generic abstraction of a weakly electric fish, a sensor line within an electric dipole is assumed as shown in figure 4. The emitter dipole is represented by circles marked with + for the positive (red) and − for the negative (blue) emitter. The sensor line is shown in green and consist of n sensors with a spacing of 5 mm. Each sensor measures the potential of the electric field. The potentials on the sensor line are calculated by equation (27). If a round object is placed in the electric field the sensors will measure a different potential than without an object, because of the field distortion of that object.

Differential measurement of electric potentials

Electric potential can be measured with respect to reference electrodes in the distance, assuming that this distant electrode has a "neutral" potential according to the measurement task. This measurement is called unipolar. It is also possible to select one specific sensor on the sensor line as a reference electrode during a unipolar measurement. This would raise the question of which sensor would make the most suitable reference. However, these challenges can be easily overcome by using differential measurements instead, which do not require reference electrodes. In real measurement situations, differential measurements have the advantage of common mode rejection which generally allows for larger gains in the amplifiers. In this work, potential differences are measured between direct neighbors on the sensor line. As shown in figure 4, this results in $n-1$ differential pairs $s_2 - s_1, s_3 - s_2, \cdots, s_n - s_{n-1}$ if n electrodes are placed along the sensor line. The direct neighborhood of two electrodes results in a potential difference $V_{2,1}, \cdots, V_{n,n-1}$ that can be assigned to a location on the sensor line between the two sensors of a differential pair. Therefore, the potential difference V can be plotted over the sensor line (voltage profile) As will become clear below, this form of voltage profile also allows the derivation of characteristics for the definition of parallax (see peak trace (PT) in section 3).

2.4. Advanced signal characteristics based on differential measurements

Each electric field, undistorted or distorted by an object, leads to a one-dimensional measurement profile on the sensor line. The undistorted field leads to an offset voltage profile from which the pattern of the distorted field deviates. Both, profile offset and distorted profile, are characteristic for a) shape and orientation of the electric source field and b) for shape and position of an object.

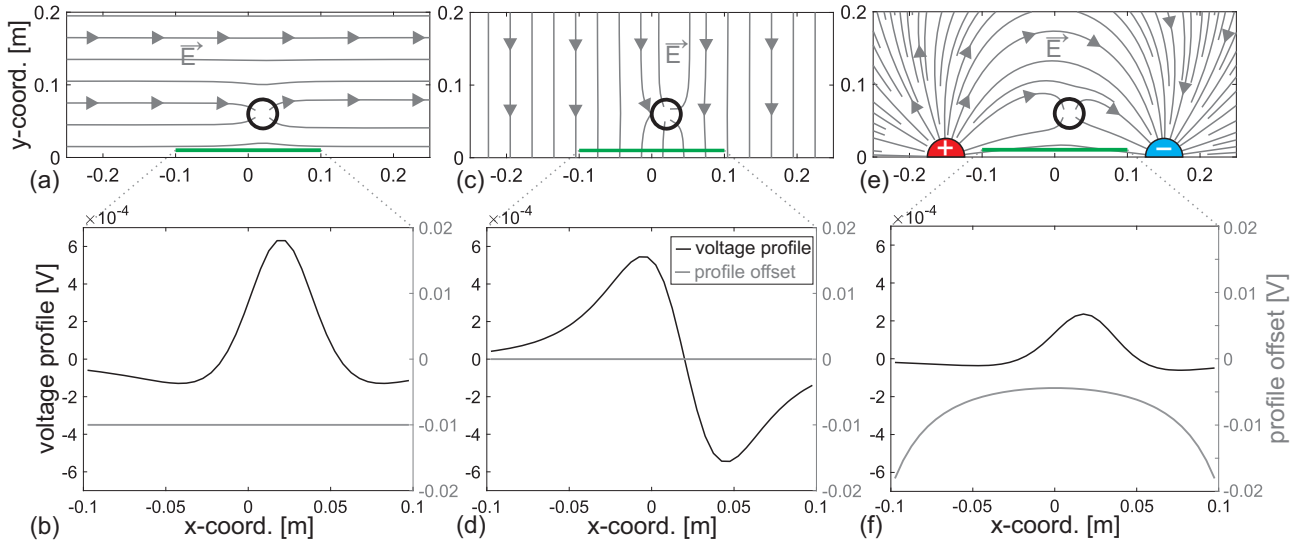

Figure 5. Object distortion and the resulting potential over the sensor line (green) for three different electric field shapes. The object position ($x = 0.02\,\mathrm{m}$, $y = 0.06\,\mathrm{m}$) and the sensor line position ($x = \pm 0.1\,\mathrm{m}$, $y = 0.01\,\mathrm{m}$), as well as the object size (radius $= 0.02\,\mathrm{m}$) is the same for all field simulations. The object is a perfect conductor and the surrounding material is water ($\epsilon_r = 81$). Additionally, the voltage profiles (black) of the distortion and the profile offsets (grey) of the individual field shape are shown in the lower figures. In (a) and (b) the results for a uniform electric field $E = 2\,\mathrm{V\,m^{-1}}$ in parallel to the sensor line is shown. (c) and (d) show a uniform electric field $E = 2\,\mathrm{V\,m^{-1}}$ vertical to the sensor line. In (e) and (f) an electric dipole field with $\pm 1\,\mathrm{V}$ at $x = \pm 0.15\,\mathrm{m}$ and its distortion is shown.

In this section, the voltage profile of the sensor line is shown exemplary for three different source field shapes/orientations and a round object, as illustrated in figure 5. Figure 5 shows the voltage patterns of the sensor line on the lower panels for the electric fields in the respective upper panels. The voltage patterns were calculated based on equation (25) and (27) in Matlab 2020b (The Mathworks Inc., Natick, MA, USA).

The horizontal orientation of the uniform electric field in figure 5(a) and the vertical orientation of the uniform electric field in figure 5(c) together with the respective voltage profiles in figure 5(b,d) serve as references to better understand the course of the voltage profile for the electric dipole field as shown in figure 5(f). The voltage profile of the electric dipole is a mixture (superposition) of figure 5(b) and (d) and depends on sensor as well as object position and the resulting field distortion.

For all following considerations, a perfectly conducting object ($\chi = 1$) with radius 0.02 m is placed at (0.02 m, 0.06 m) above the sensor line. The round object is laterally displaced by 20 mm from the center of the sensor line along the x-axis. The surrounding medium is water ($\epsilon_r = 81$) and the conducting object creates a field distortion which is measured at individual locations on the sensor line. The sensor line has a length of 0.2 m with $n = 40$ sensors placed 5 mm apart from each other.

First, a uniform electric field with $E = 2\,\mathrm{V\,m^{-1}}$ in parallel to the sensor line is considered (figure 5(a)). The parallel field lines and the equipotential lines perpendicular to them (not shown) result in a voltage across the sensor line as shown in figure 5(b). The characteristic feature of the field distortion is a local maximum (peak) at the object position ($x = 0.02\,\mathrm{m}$) on the sensor line. The voltage profile without an object (profile offset) is also shown in figure 5(b) as a grey line.

If the uniform electric field with $E = 2\,\mathrm{V\,m^{-1}}$ is rotated by 90° (figure 5(c)), the field lines meet the sensor line perpendicularly and the equipotential lines run parallel to the sensor line. The distorted potential across the sensor line, as shown in figure 5(d), has a local maximum and a local minimum. The inflection point of the voltage profile corresponds to the object position ($x = 0.02\,\mathrm{m}$) above the sensor line. Thus, the local minimum, local maximum and the inflection point are characteristic of a perpendicular uniform electric field. By suitable sensor placement, the offset voltage profile of the initial field across the sensor line results to zero. Therefore, the object distortion can be identified easier.

If an electric dipole field is generated instead of the uniform electric field the sensor line is placed between the two emitters (figure 5(e)). The two emitter poles $\pm 1\,\mathrm{V}$ are located at $x = \pm 0.15\,\mathrm{m}$. The distance of 0.05 m between the two emitters and the sensor array is chosen so that outer sensors on the sensor array are not influenced by the two emitters too strongly. As shown in figure 5(f), a characteristic bell-shaped curve with

a local maximum (peak) corresponding to the object position ($x = 0.02\,\mathrm{m}$) is obtained.
For the field distortion of the round object in a dipole field, a combination of the voltage profiles shown in figure 5(a) and 5(c) is expected. Since the electric field close to the object is parallel to the sensor line, the voltage profile is similar to that of the uniform field in figure 5(a,b). If the object is placed above a pole, the electric field lines run perpendicular to the sensor line and the voltage profile is similar to that in figure 5(c,d). However, the offset of the voltage profile (grey) in figure 5(f) is nonlinear as apposed to constant offset profile of figure 5(a,c).

3. Scanning strategies for distance and direction estimates of objects based on parallax

Based on the previous observation of the electric field characteristics with the field distorted by a round, conductive object, different scanning strategies can be established for distance and direction (vertical distance, lateral displacement) estimation. The effect of motion parallax in context of electric field imagery is illustrated by the example of an active movement of the sensor line.
As a basis for the definition of parallax, a characteristic property of the voltage profile during a relative movement of sensor line and object is introduced. This is the peak trace (PT), which is defined in the following. If the voltage profile $V(x)$ – with x being a position on the sensor line – has a maximum at position x_{peak} and this maximum lies in the interior of the voltage profile, i.e.

$$V(x_{\mathrm{peak}}) \geq V(x) \quad \forall x \in \text{sensor line}, \tag{28}$$

then this voltage profile is considered to have a peak at this position. If $V(x)$ was a smooth function then the position of the possible peak would be located at

$$x_{\mathrm{peak}} = \arg\max_x V(x) \tag{29}$$

and the local course of the function at the peak would have to be convex:

$$\exists x_{\mathrm{peak}} \wedge V'(x_{\mathrm{peak}}) = 0 \wedge V''(x_{\mathrm{peak}}) < 0 \tag{30}$$

When the sensor line moves past an object, a peak appears in the voltage profile, changes its position in the voltage profile and disappears again. The imaginary trace (distance) that the peak leaves on the sensor line during the observed sensor movement is defined as the peak trace (PT).

$$\mathrm{PT} = |x_{\mathrm{peak,\ last\ observation}} - x_{\mathrm{peak,\ first\ observation}}| \tag{31}$$

Figure 6 visualizes several aspects of the PT. An object is placed at (0 m, 0.04 m) and the sensor moves from left to right along the x-axis (see figure 6(a)). It is

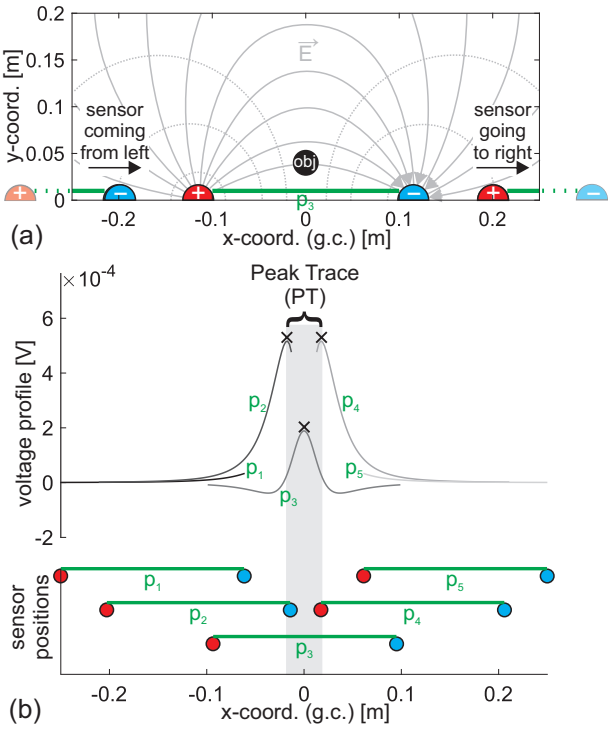

Figure 6. Illustration of the peak trace (PT). For a long sensor movement in x-direction (a), the PT can be defined as the imaginary trace left by a local maximum (peak) on the sensor line during the relative movement of sensor and object. At sensor position p_1 and p_5 no peak is detected in the upper panel of (b). The first peak is fully formed at p_2 and disappears again at p_4 (each marked with a x), resulting in the peak trace (PT) in global coordinates (g.c.), as shown in (b). The vertical offset of the sensor line positions (p_1 to p_5) in the lower panel of (b) serves illustration purposes only.

assumed that the sensor position in world coordinates is known. The permanently measured voltage profile on the sensor line due to the field distortion is shown in figure 6(b) for five different sensor positions (p_1 to p_5) on the x-axis. As the initial field is an electric dipole field, the maximum (peak) can be traced, once it has fully formed (p_2) until it disappears again (p_4). At sensor position p_1 and p_5 no peak is detected. The resulting width of the PT is also marked with a curly bracket in figure 6(b). With the help of the PT width parallax observation can be done for distance and direction estimations.
Based on this, different scanning strategies (sensor line movements) are investigated, which on the one hand vary between long and short movements and on the other hand address the influence of known and unknown sensor line positions. A long sensor movement is a movement whose length is not known a priori, but which must go far enough so that a complete PT is measured (complete in this case means that the peak appears after the start of the measurement and disappears before the end of the measurement).

If equation (32) holds true, the movement can be interpreted as a long sensor movement.

$$\neg\exists\,\mathrm{peak}_{\text{start pos.}} \;\wedge\; \neg\exists\,\mathrm{peak}_{\text{end pos.}} \;\wedge\; \exists\,\mathrm{PT} \tag{32}$$

A short sensor movement is a movement that is determined a priori (in this case one sensor line length). If a peak occurs, its PT can always be used because a unique object position can be derived based on the known movement length. A global coordinate (g.c.) system is used when assuming that the sensor position is known, while local coordinate (l.c.) system (attached to the sensor line) is used when assuming that the sensor position is unknown. The sensor motion and its corresponding PT is shown for known and unknown sensor positions (cf. figure 7). For a dynamic visualization of the movement strategies, please see the supplementary video files. For all movement strategies, the effect of parallax can be shown no matter if the object itself is moving or the active sensor is moving relative to the object.
The results for the individual scanning strategies were simulated in Matlab 2020b.

3.1. Long sensor movements with known sensor positions

In this scenario, it is assumed that the position of the moving sensor is known in a global coordinate system and that no peak is detected at the sensor start and end positions. Hence, a peak is only detected while the sensor moves. Therefore, the movement starts far to the left of the object to be scanned and ends far to its right, to ensure that the peak can be completely measured on the sensor line, as described in equation (32). The object that is placed at $x = 0.02\,\mathrm{m}$ in different vertical distances (y-coord., p_1 to p_8) generates different PTs during the long sensor movement (7(b), shaded in grey). If the object is placed farther away, the PT width is larger than for closer objects. Thus, a relationship between the PT width and the vertical distance (y-coord.) from the sensor line to the object can be established.
In addition, the center of the PT is evaluated, as indicated by the triangles in figure 7(b). For all different vertical distances the center of PT corresponds with the x-coordinate of the object. Therefore, the vertical distance and direction (lateral displacement) of the object in global coordinates can be estimated by the PT and its center by a long sensor movement with known sensor positions.

3.2. Long sensor movement with unknown sensor positions

In this scenario, the sensor movement is the same as in section 3.1 but it is assumed that the global position of the sensor during its movement remains unknown. Thus, the PT can only be measured in the local coordinate system on the sensor line. The object is placed at $x = 0.02\,\mathrm{m}$ in different vertical distances (y-coord.). The width of the PTs are the same, independent of the vertical object distance to the sensor line (figure 7(c)). However, a PT with the length of the sensor line can not be used for distance and direction estimation. Therefore, this strategy is not further pursued.

3.3. Short sensor movement with known sensor positions

Inspired by the biological model, in this scenario, a short sensor movement with globally known sensor positions is performed. The center of the sensor line is moved forward by one sensor line length from $-0.1\,\mathrm{m}$ to $0.1\,\mathrm{m}$ on the x-axis in global coordinates. The object that is placed at different vertical distances (y-coord., p_1 to p_8) generates different PTs through the short sensor movement, as shown in figure 7(d). Closer objects will generate a shorter PT width than objects that are placed farther away. Thus, a relationship between the PT width and the vertical distance to the object can be established for this short sensor movement. It must be pointed out that the widths of the PTs differ from those of the long movements.
Throughout these short movements the centers of the PTs, as shown by triangles in figure 7(d), do not correspond to the lateral displacement (x-coord.) of the object. Closer examination shows that a systematic shift of the PT center is recognizable.
As a consequence, additional features are needed to estimate the vertical distance and lateral displacement of the object for a short sensor movement correctly. Therefore, figure 8 shows the different situations in (a) with the relevant voltage profiles in (b) to (e). With the help of the voltage profiles a feature is developed to choose whether a PT is valid or not. In figure 8(a) the objects are not only placed at different vertical distances (y-coord.) but additionally with a lateral displacement (x-coord.). For an object that is placed at $(-0.12\,\mathrm{m},\ 0.04\,\mathrm{m})$ the measured voltage profile is shown in figure 8(b). A local maximum (peak) is only detected at position p_1 of the sensor line, for all other sensor positions (p_2, p_3) no local maximum can be detected. Therefore, the maximum (peak) is only detectable during a part of the movement. As a consequence, the PT is invalid. In this case, the lateral displacement of the object was too far to the left to be properly detected. Figure 8(c) shows a valid PT for an object placed at $(0\,\mathrm{m},\ 0.04\,\mathrm{m})$, because all sensor positions detect a local maximum (peak) in the voltage profile. If the object is placed at $(0.04\,\mathrm{m},\ 0.04\,\mathrm{m})$ or $(0.08\,\mathrm{m},\ 0.04\,\mathrm{m})$ the PT is also invalid, because no

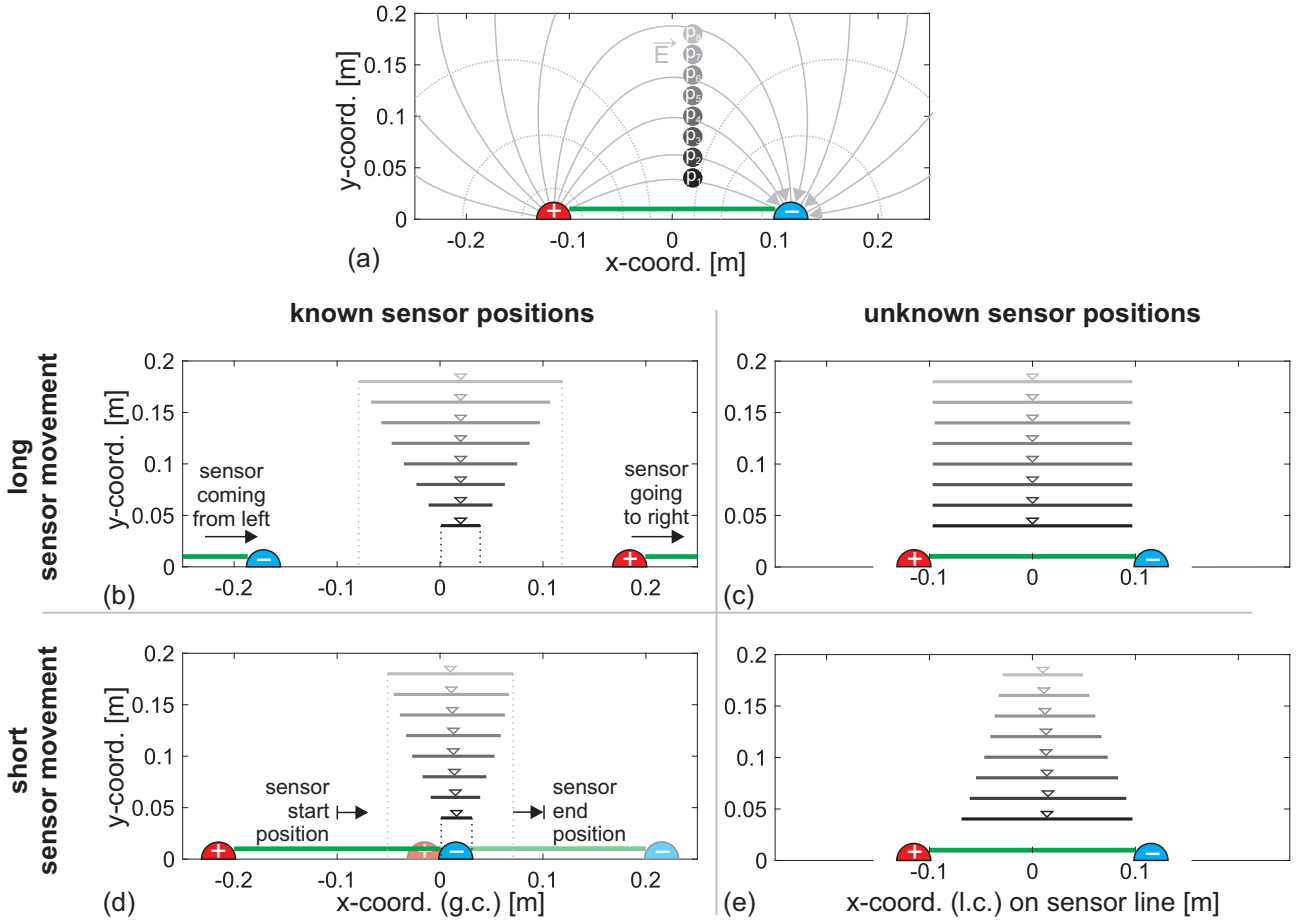

Figure 7. Four different scanning strategies for distance (vertical distance) and direction (lateral displacement) estimation. The perfectly conducting object is placed at $x = 0.02\,\mathrm{m}$ at different vertical distances (p_1 to p_8) from the sensor line (green), as shown in (a). The PTs for the scanning strategies are shown in (b) to (e) in different shades of grey (closest distance p_1 dark grey, furthest distance p_8 light grey). The center of the PT is marked by a triangle. A global coordinate (g.c.) system is used for the scanning strategies with known sensor positions and a local coordinate (l.c.) system is used for the unknown sensor positions.

local maximum (peak) is detected at position p_1 of the sensor line, as shown in figure 8(d, e).

In summary, a PT is invalid if the voltage profile contains a maximum (peak) at the sensor start position and none at the sensor end position or vice versa. This occurs when the sensor start or end position are too close to or directly underneath an object. PTs are valid if the long movement starts "far enough" to the left of the object and ends "far enough" to the right, as shown in figure 7(b), or the short sensor movement starts and ends with a local maximum (peak).

Therefore, the vertical distance and direction (lateral displacement) of the object in global coordinates can be estimated by a valid PT and its center by a short sensor movement with known sensor positions.

3.4. Short sensor movement with unknown sensor positions

As a fourth scanning strategy the sensor performs a short movement without knowledge of the sensor positions. For an object that is placed at $x = 0.02\,\mathrm{m}$ at different vertical distances (y-coord.) the resulting PT is shown in figure 7(e). In contrast to the other scanning strategies, closer objects generate a larger PT width than objects that are farther away. The x-position of the local maximum (peak) are measured in local coordinates on the sensor line due to the unknown sensor positions. Since the object is not centered, the centers of the PTs do not match the x-coordinate of the object position (lateral displacement), as illustrated by triangles in figure 7(e).

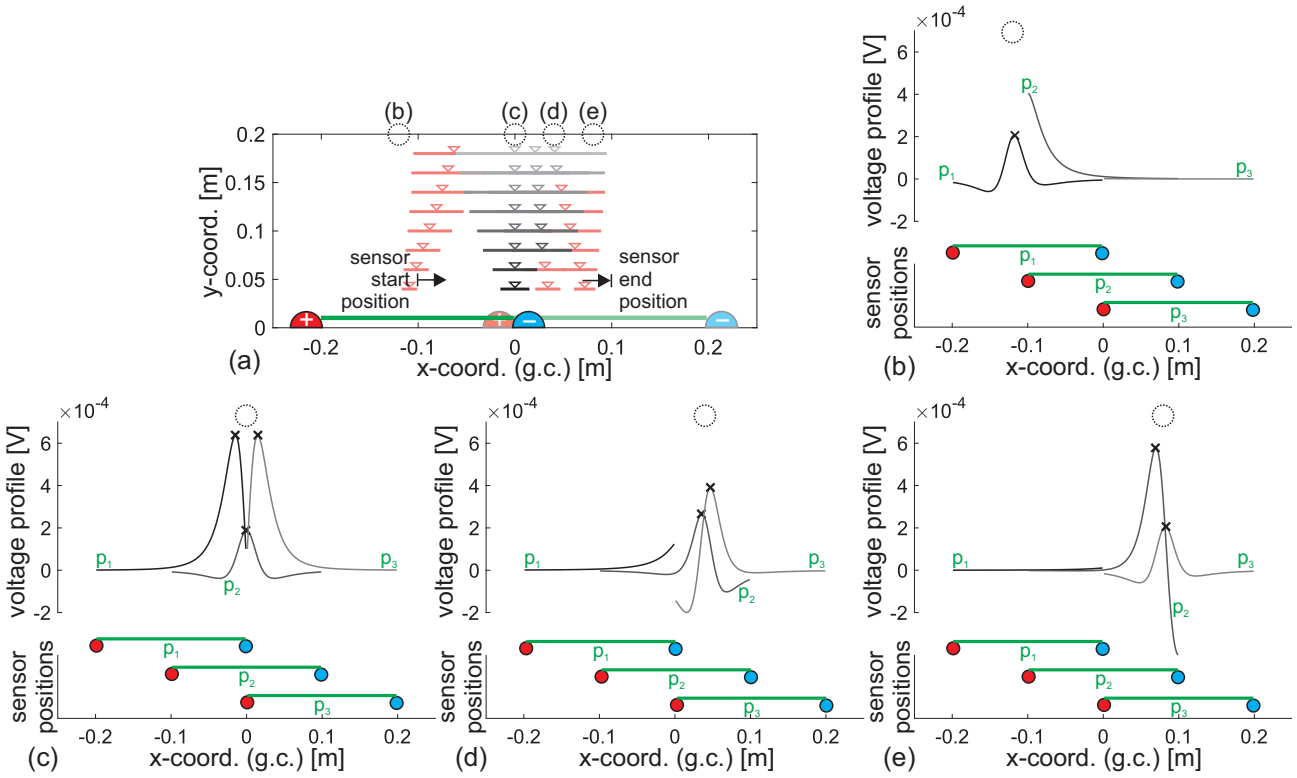

Figure 8. Illustration of a short sensor movement with known sensor positions for four different objects. Additional features (when is a PT valid/invalid?) are needed to estimate the vertical distance and lateral displacement of the object correctly. Therefore, objects are placed at $x = -0.12\,\mathrm{m}$ (b), $x = 0\,\mathrm{m}$ (c), $x = 0.04\,\mathrm{m}$ (d) and $x = 0.08\,\mathrm{m}$ (e) at a constant vertical distance of 0.04 m from the sensor line. The sensor line is drawn for three different horizontal positions (p_1 to p_3) during a short sensor movement (vertical offset of sensor line positions for visual illustration only). (a) shows the width of the PTs for (b-e) in the bottom row. Red PTs are invalid due to the fact, that in (b) only the first sensor position (p_1) detects a local maximum and in (d), (e) only position p_2 and p_3. Valid PTs are shown in black and grey and results from (c), where all three sensor positions detect a local maximum (peak) or the first (p_1) and last (p_3) detects no maximum (peak).

3.5. Field of view for the different sensor movements

Similar to visual systems, a field of view can also be defined for the perception of objects in an electrical vision system. For objects located within the aperture angle of this field of view, the lateral displacement and vertical distance can be determined, as shown in figure 9 for the different scanning strategies. The aperture angle and the field of view result indirectly from the valid object positions. Valid object positions are those that lead to a complete - i.e. valid - peak trace (PT) on the sensor when the scan movement is performed (section 3.3 and 3.4).

For a long sensor movement with known sensor positions the field of view for the sensor used amounts to 56°, as shown in figure 9(a). For a given vertical distance of an object in y-direction and a sensor motion starting far to the left, the beginning of a PT appears on the sensor from the position marked with a cross and ends at the second cross in the same line as the motion continues. The two crosses therefore mark the ends of the PT for a given object position (circles in figure 9). The set of crosses form a triangular shape whose opening angle can be understood as a field of view. (figure 9(a)). For long sensor movements, the question of whether an object is valid or invalid recedes to the background, since any object can be made valid if the sensor movement is only made long enough.

Long sensor movements with unknown sensor positions lead to PTs which cover the full length of the sensor (equal length of grey lines in figure 7(c)) and hence do not allow any conclusion about object positions (vertical distance, lateral displacement). Therefore, figure 9(b) is left empty.

The field of view for the short sensor movement, as shown in figure 9(c, d), amounts to 53° for the known and unknown sensor positions. The field of view is determined using valid PTs and the associated objects as detailed above. The maximal detected PT length is a bit wider than the field of view, as indicated by two black crosses in each line in figure 9(c, d).

The small difference in the field of view between the different scanning strategies results from the small sensor movement of only one sensor length (0.2 m), that

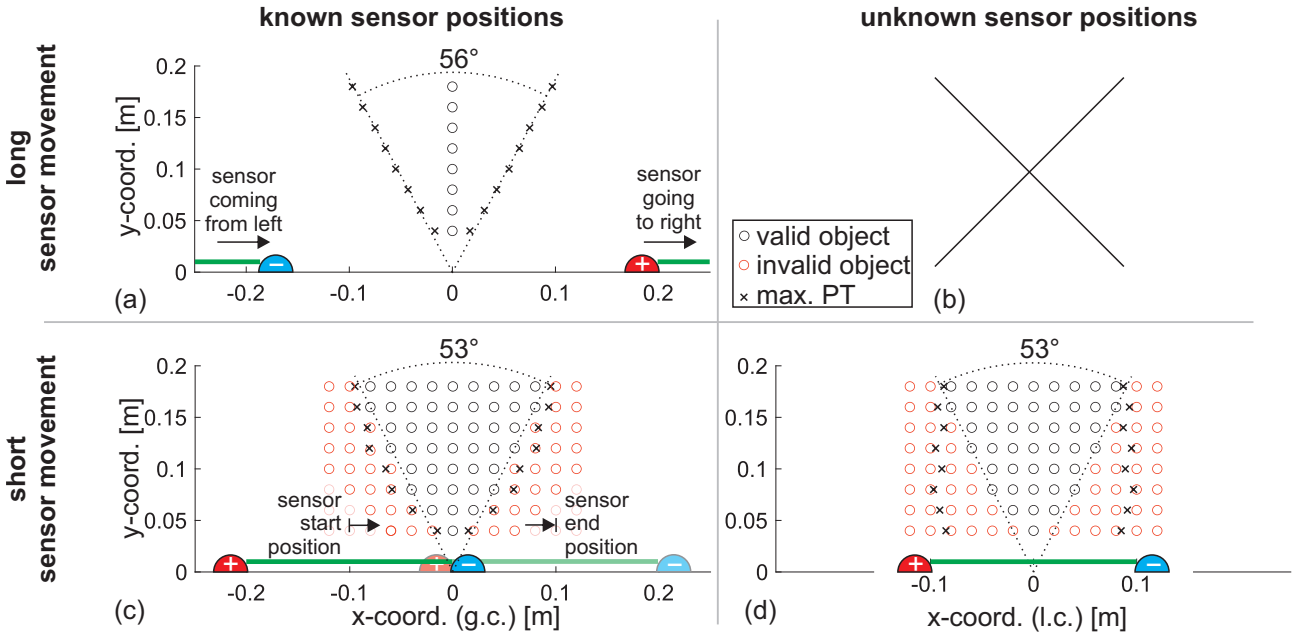

Figure 9. Field of view for the different scanning strategies. The long sensor movement with known sensor positions in (a) has a 56° field of view. The maximal PT length, i.e. the first and last occurrence of a maximum (peak) on the sensor, is marked with a cross in each line. The long sensor movement with unknown sensor positions (b) has no field of view due to the fact that all PTs have the same length (equal length of grey lines in figure 7(c)). The short movements in (c) and (d) have a field of view of 53°, which can be determined by a valid PT (black cross) and corresponding valid object positions (black circles). An invalid object is marked by a red circle.

nonetheless covers almost the full field of view of the long sensor movement. Accordingly, a smaller sensor movement will generate a smaller field of view.

4. Definition of parallax in electric field imagery

Based on the above, we now define electric parallax as the relative movement of a signal characteristic of the voltage profile (here, the maximum or peak of the curve, see figure 6) that travels along the sensor line as a result of an object or sensor movement (figure 7).

The length of the PT, resulting from an object distortion of an originally dipole-shaped field, varies for different object distances (vertical distance). An analogy to the emergence of optical parallax in an imaging system can be formulated in such a way that the basic shape of the electric field, detuned by a given object, determines the shape and extent of the voltage profile on the sensor line and thus acts like a lens.

Another analogy to motion parallax is the fact that objects will appear larger if they are closer to an observer and smaller at a larger distance. The movement of the characteristic maximum (peak) along the sensor behaves the same way. Closer objects generate wider PTs than objects at larger distances. This also holds true for short sensor movements with unknown sensor positions, as shown in figure 7(e).

If the sensor positions are known, as in figure 7(b, d), the PTs correlate with the vertical distances, i.e. larger distances lead to wider PTs.

Figure 10 shows, column by column, the determination of vertical distance and direction (lateral displacement) of objects for three different motion conditions. Based on knowledge of the width of a PT and the position of the PT center (in global or local coordinates), the vertical distance (y-coord.) and lateral displacement (x-coord.) of an object can be determined. A large sensor movement with known sensor positions exhibits a dependency between the PT width and vertical distance (y-coord.) of the object position (figure 10(a)) and the PT center and lateral displacement (x-coord.) of the object position (figure 10(b)).

Short movements with known sensor positions also show a dependency between the PT width and vertical distance (y-coord.) of the object for valid PTs at close range, as shown in figure 10(c). If the objects are farther away the valid PT widths spread horizontally. Although these objects have the same vertical distance they generate PT widths of different length leading to the wrong assumption that they are situated at different vertical distances (referred to as *deviation* in figure 10(c)). Due to this horizontal spread, an additional ambiguity occurs which results in objects of different distances having the same PT width (referred to as *ambiguity* in figure 10(c)). However, the PT

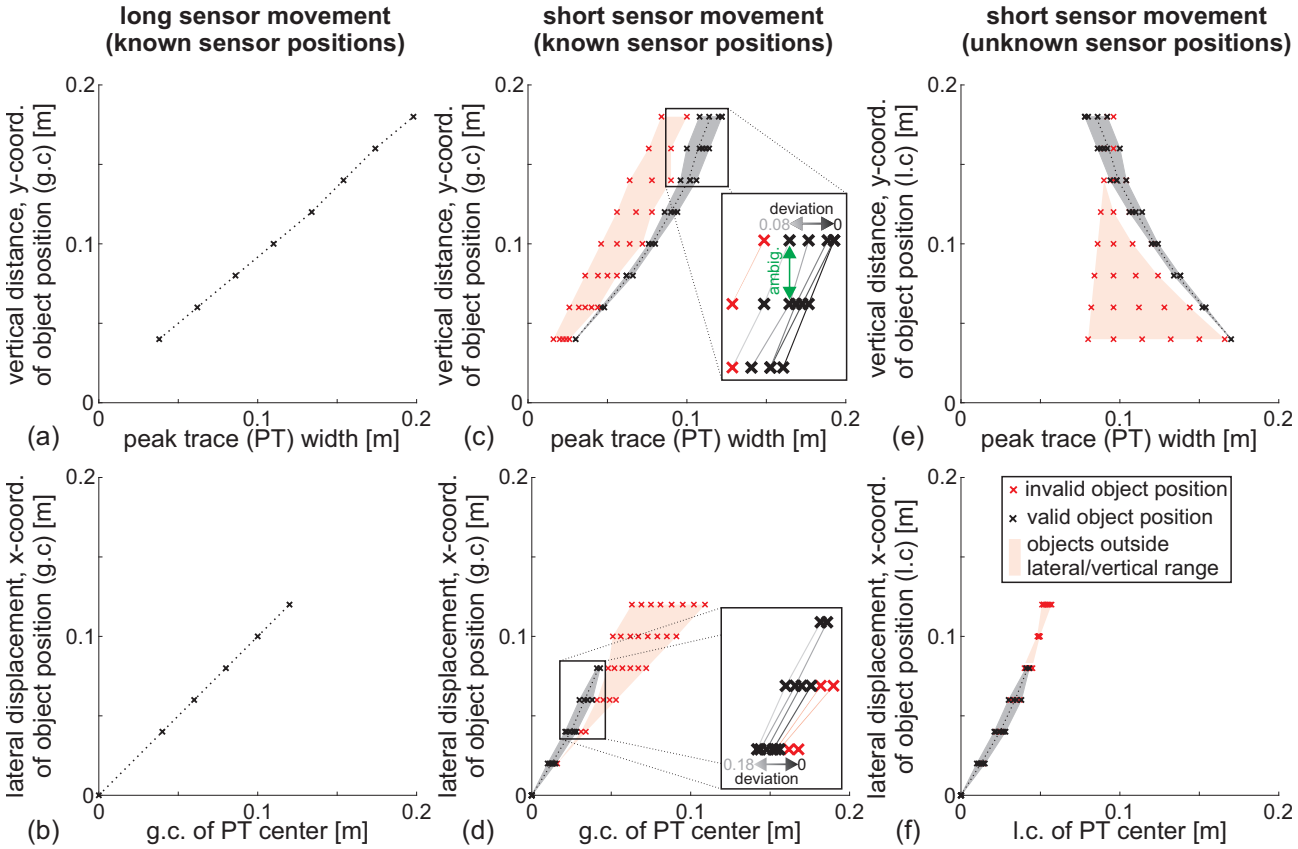

Figure 10. Results of the distance and direction (vertical distance, lateral displacement) estimation for different scanning strategies. The relation between PT width and vertical distance (y-coord. of object position) is shown as a dotted line for a long sensor movement in (a). Also the relation between PT center and lateral displacement (x-coord. of object position) is shown as a dotted line in (b). The short sensor movements with known sensor positions are shown in (c) and (d). For distant objects the PT width spread horizontally. The red positions are invalid according to the condition for valid PTs and therefore, outside the lateral/vertical range of the sensor line. In (e) and (f) short sensor movement with unknown sensor positions are shown.

center is unique if only the valid PTs are considered (figure 10(d)). Although these valid objects have the same lateral displacement, they create different PT center positions leading to the wrong impression that they are situated at different lateral displacements (referred to as *deviation* in figure 10(d)). Both deviations can be associated with a concept of blur or rather, when regarded in a complementary way), acuity. With this short sensor movement the field of view (see figure 9(c)) is limited and therefore, no objects outside the lateral range can be estimated, if the lateral displacement (x-coord. of object position) is wider than 0.08 m (figure 10(d)).

For a short sensor movement with unknown sensor positions the PT width and the vertical distance (y-coordinate of the object position) are correlated if valid PTs are considered. With increasing vertical distance, the resolution of valid objects declines (figure 10(e)). The PT center correlates with the lateral displacement (x-coordinate of the object position) and is again limited through the field of view by the valid PTs and their center.

In summary, for a long sensor movement with known sensor positions the estimation of object position (vertical distance, lateral displacement) is conducted with the PT width and its center. For a short sensor movement the object position should be located directly above the area that is covered by the sensor during its active sweep motion to get valid PTs and therefore a correct estimation of the object position.

5. Discussion

This work uses Mormyrid weakly electric fish as a biological inspiration. These fish utilize a self-generated electric field for communication with conspecifics and active electrolocation of nearby objects. The emitted dipole-like electric field is detected via specialized electroreceptors distributed across the fish skin [8].

Pedraja *et al* [11] verified that electric fish use a speed-based cue for distance perception when centering

between two moving plates in a shuttle tracking task. This speed-based cue is comparable to visual motion parallax. It was shown that the length that the electric image travels along the skin (Δ_{image}) when the fish swims by an object depends on the lateral distance to the object, even when the actual translation (Δ_{object}) is constant. The ratio between the image and the actual translation (IOR = $\Delta_{image}/\Delta_{object}$) was shown to provide distance information.

In this work the weakly electric fish is abstracted as an electric dipole with a sensor line between the two emitters. Based on this reduced example, the question is asked, how an object is localized by an active electrical sensor system based on parallax. This question has already been tackled based on probabilistic (Bayes filter) or model-based (Kalman filter) approaches [25, 26, 27]. It has already been shown that approaches using basic field features achieve high localization accuracy and in turn can serve as features for further processing stages. Examples are localization methods based on contour-rings of rotated and linearly shifted EEVs (ensembles of electrosensory viewpoints) [28, 29].

The main goal of the current work was a transfer of the parallax concept from geometrical optics to the field of electrolocation or electric field imagery in general. In order to keep the simulation environment as lean as possible, this work did not rely on a full FEM simulation but on an analytical description of a round object in a dipole field following Rasnow [12] with the simplifying assumptions that the object is small and the field is uniform in its close vicinity.

Based on this, the voltage profile along an imaginary sensor line can be determined. The voltage profile is the spatial sequence of the voltage differences of neighboring sensor points of the sensor line. In the presence of an object, the voltage profile shows a maximum (peak), which moves along the sensor line during an active sensor motion. The spatial width of the motion of this peak, i.e the width of the peak trace (PT), and the location of its center on the sensor line are sufficient to determine the position (vertical distance, lateral displacement) of an object. For a short sensor movement with unknown sensor positions the PT behaves the same as for instance the displacement of an object image on the retina of an eye or on the sensor surface of an optical camera. Close objects generate a larger PT width than more distant objects. Therefore, the electrical parallax defined in this way is the direct correlate to the optical parallax and can be used for depth perception. Importantly, the basic shape of the underlying electric field (dipole in the case investigated here) determines the measurable effects of the field de-tuning by an object on the sensor line and therefore acts like a lens. With respect to the biological template, where the body shape as well as the anatomy of the electric organ are variable across species, that morphological pre-receptor mechanisms can direct affect how these fish make use of the electric field [e.g. 30].

Additional scanning strategies for the estimation of the object position (vertical distance, lateral displacement) were also introduced in this work.

A long sensor movement with known sensor positions leads to a clear dependency for an object position as summarized in equation (33).

$$\text{Object position} = \begin{cases} \text{PT width} & \text{for vertical dist.} \\ \text{PT center} & \text{for lateral disp.} \end{cases} \quad (33)$$

Given a known sensor position, a short PT width results to an object near the sensor line and a large PT to a more distant object. This observation seems to be opposite to the effect observed in optical parallax.

A short sensor movement with known sensor positions needs additional features to test whether a PT is valid. Therefore, the first and last position of the sensor movement is evaluated for a local maximum (peak). The PT is invalid if the voltage profile contains a maximum (peak) at the sensor start position and none at the sensor end position or vice versa. By this condition, only objects located directly above the area that is covered by the sensor during its active sweep motion are correctly estimated.

The relation between valid and non valid PTs with distance and length of the sensor movement sweep offer an interesting link to the biological template: So-called B-scans have been implicated in spatial learning and distance measurement in weakly electric fish [9]. It will be interesting to study the relation of the amplitude of these B-scans with object properties, nearness of the object and quality of the distance estimate obtained by the fish.

This work focused on the object localization of a individual object. If additional objects occur simultaneously, for example in a symmetrical arrangement with different object sizes, the overlapping electric field distortions might lead to incorrect distance and direction estimates of the active sensor. In a more general and natural situation where objects enter the field of view of the active sensor one by one, a system at a higher processing level could take into account for the object tracking, to solve this problem at least partially.

The next steps will be to generate a more complex model of the weakly electric fish to understand the natural scanning behaviour as investigated in [31]. Therefore, the movement of the Schnauzenorgan and the tail will be considered. Raising the complexity also means to put the shape of the body and thus the shape of the sensor into the focus. That means to utilise curved 2D sensor arrays in 3D space. This is closely related to

a series of studies in *Gymnotus carapo*, showing the strong dependence of the electric field on these parameters (for an overview for Gymnotus, see [32]). In addition, a physical implementation as a reference is planned in a next step.

Acknowledgments

This work has been supported by the Deutsche Forschungsgemeinschaft (DFG, German Research Foundation) - ref. no. SCHN 1339/4-1, EN 826/8-1

References

[1] Hermann Von Helmholtz. *Helmholtz's treatise on physiological optics*, volume 3. Optical Society of America, 1925.

[2] E Bruce Goldstein and James Brockmole. *Sensation and perception*. Cengage Learning, 2016.

[3] Mandyam V Srinivasan and Svetha Venkatesh. *From living eyes to seeing machines*. Oxford University Press, 1997.

[4] Andreas B Sichert, Robert Bamler, and J Leo van Hemmen. Hydrodynamic object recognition: when multipoles count. *Physical review letters*, 102(5):058104, 2009.

[5] Gerhard von der Emde and Steffen Fetz. Distance, shape and more: recognition of object features during active electrolocation in a weakly electric fish. *Journal of Experimental Biology*, 210(17):3082–3095, 2007.

[6] MICHAEL VL Bennett. Electroreception. In *Fish physiology*, volume 5, pages 493–574. Elsevier, 1971.

[7] Angel Ariel Caputi and Ruben Budelli. Peripheral electrosensory imaging by weakly electric fish. *Journal of Comparative Physiology A*, 192(6):587, 2006.

[8] Mark E Nelson and Malcolm A Maciver. Prey capture in the weakly electric fish apteronotus albifrons: sensory acquisition strategies and electrosensory consequences. *Journal of Experimental Biology*, 202(10):1195–1203, 1999.

[9] James J. Jun, André Longtin, and Leonard Maler. Active sensing associated with spatial learning reveals memory-based attention in an electric fish. *Journal of Neurophysiology*, 115(5):2577–2592, 2016.

[10] M. J. Toerring and P. Belbenoit. Motor programmes and electroreception in mormyrid fish. *Behavioral Ecology and Sociobiology*, 4(4):369–379, 1979.

[11] Federico Pedraja, Volker Hofmann, Kathleen M Lucas, Colleen Young, Jacob Engelmann, and John E Lewis. Motion parallax in electric sensing. *Proceedings of the National Academy of Sciences*, 115(3):573–577, 2018.

[12] Brian Rasnow. The effects of simple objects on the electric field of apteronotus. *Journal of Comparative Physiology A*, 178(3):397–411, 1996.

[13] H. W. LISSMANN and K. E. MACHIN. The Mechanism of Object Location in Gymnarchus Niloticus and Similar Fish. *Journal of Experimental Biology*, 35(2):451–486, 06 1958.

[14] R. Budelli and A.A. Caputi. The electric image in weakly electric fish: perception of objects of complex impedance. *Journal of Experimental Biology*, 203(3):481–492, 02 2000.

[15] Chen L, House JL, Krahe R, and Nelson ME. Modeling signal and background components of electrosensory scenes. *J Comp Physiol A*, 191:331–345, 2005.

[16] Miyoung Sim and DaeEun Kim. Electrolocation based on tail-bending movements in weakly electric fish. *Journal of Experimental Biology*, 214(14):2443–2450, 07 2011.

[17] A A Caputi, R Budelli, K Grant, and C C Bell. The electric image in weakly electric fish: physical images of resistive objects in Gnathonemus petersii. *Journal of Experimental Biology*, 201(14):2115–2128, 07 1998.

[18] C. Assad, B. Rasnow, and P.K. Stoddard. Electric organ discharges and electric images during electrolocation. *Journal of Experimental Biology*, 202(10):1185–1193, 05 1999.

[19] Walter heiligenberg. Theoretical and experimental approaches to spatial aspects of electrolocation. *Journal Comp Physiol. A*, 103:247–272, 05 1975.

[20] David Babineau, Andre Longtin, and John E. Lewis. Modeling the electric field of weakly electric fish. *Journal of Experimental Biology*, 209(18):3636–3651, 09 2006.

[21] Gerhard von der Emde. Distance and shape: perception of the 3-dimensional world by weakly electric fish. *Journal of Physiology-Paris*, 98(1):67–80, 2004. Representation of 3-D Space Using Different Senses In Different Species.

[22] Y. M. Fujita, K.and Kashimori. Modeling the electric image produced by objects with complex impedance in weakly electric fish. *Biol Cybern*, 103:105–118, 2010.

[23] Paul L. Nunez and Ramesh Srinivasan. *Electric Fields of the Brain: The Neurophysics of EEG*. Oxford University Press, USA, 2 edition, 2005.

[24] John David Jackson. *Classical electrodynamics*. John Wiley & Sons, 2007.

[25] Vincent Lebastard, Christine Chevallereau, Alexis Girin, Noël Servagent, Pol-Bernard Gossiaux, and Frédéric Boyer. Environment reconstruction and navigation with electric sense based on a kalman filter. *The International Journal of Robotics Research*, 32(2):172–188, 2013.

[26] Yang Bai, James Snyder, Yonatan Silverman, Michael Peshkin, and Malcolm A MacIver. Sensing capacitance of underwater objects in bio-inspired electrosense. In *2012 IEEE/RSJ International Conference on Intelligent Robots and Systems*, pages 1467–1472. IEEE, 2012.

[27] Yonatan Silverman, Lauren M Miller, Malcolm A MacIver, and Todd D Murphey. Optimal planning for information acquisition. In *2013 IEEE/RSJ International Conference on Intelligent Robots and Systems*, pages 5974–5980. IEEE, 2013.

[28] Sabine Wolf-Homeyer, Jacob Engelmann, and Axel Schneider. Electrolocation of objects in fluids by means of active sensor movements based on discrete eevs. *Bioinspiration & biomimetics*, 11(5):055002, 2016.

[29] Sabine Wolf-Homeyer, Jacob Engelmann, and Axel Schneider. Application of reduced sensor movement sequences as a precursor for search area partitioning and a selection of discrete eev contour-ring fragments for active electrolocation. *Bioinspiration & biomimetics*, 13(6):066008, 2018.

[30] R. Pusch, G. von der Emde, M. Hollmann, J. Bacelo, S. Nobel, K. Grant, and J. Engelmann. Active sensing in a mormyrid fish: electric images and peripheral modifications of the signal carrier give evidence of dual foveation. *Journal of Experimental Biology*, 211(6):921–934, 2008.

[31] Volker Hofmann, Juan Ignacio Sanguinetti-Scheck, Leonel Gómez-Sena, and Jacob Engelmann. Sensory flow as a basis for a novel distance cue in freely behaving electric fish. *Journal of Neuroscience*, 37(2):302–312, 2017.

[32] M.E. Castello, P.A. Aguilera, O. Trujillo-Cenoz, and A.A. Caputi. Electroreception in Gymnotus carapo: pre-receptor processing and the distribution of electroreceptor types. *Journal of Experimental Biology*, 203(21):3279–3287, 11 2000.